Journal of Materials Chemistry A

RSC Publishing

PAPER

View Article Online
View Journal | View Issue

Cite this: J. Mater. Chem. A, 2013, 1, 2418

Highly aligned $Cu_2O/CuO/TiO_2$ core/shell nanowire arrays as photocathodes for water photoelectrolysis

Qiang Huang,[a] Feng Kang,[a] Hao Liu,[a] Quan Li[a] and Xudong Xiao*[ab]

Received 31st October 2012
Accepted 4th December 2012

DOI: 10.1039/c2ta00918h

www.rsc.org/MaterialsA

Highly aligned Cu_2O, Cu_2O/CuO, $Cu_2O/CuO/TiO_2$ and Cu_2O/TiO_2 nanowires arrays on Au substrates were prepared by controlled air annealing of the electrodeposited Cu nanowires and furthered with dip coating. Photoelectrochemical investigations were carried out to determine their potential as photocathodes for water photo-reduction. The photocurrent of the Cu_2O nanowires photocathode was found to be twice that of the Cu_2O film, largely due to the higher surface area and the shorter carrier diffusion length associated with the nanowires array configuration. However, the bare Cu_2O nanowires suffered from a significant photo-induced reductive decomposition with the electronic state of copper transferred from Cu(I) to Cu(0). By modifying the surface of the Cu_2O nanowires with protecting layers of CuO and TiO_2, direct contact of Cu_2O with the electrolyte was avoided and the $Cu_2O/CuO/TiO_2$ coaxial nanocable structures were found to gain a 74% higher photocurrent and 4.5 times higher stability, compared with the bare Cu_2O nanowires array. To understand the mechanism of the improved performance, a detailed characterization and analysis on the structure, circuitry and band alignment for the $Cu_2O/CuO/TiO_2$ configuration was carried out. The present study suggests a promising nanostructured photocathode configuration, which can lead to a large photocurrent with good stability against photocorrosion.

Introduction

With the aim of creating a clean and sustainable energy supply, the direct use of solar energy to produce chemical energy has been pursued for many years.[1–5] Particularly, the photoelectrolysis of water to generate hydrogen by semiconductor photoelectrodes has attracted great attention because of its advantage of using only water and sunlight, both of which are widely distributed as raw materials.[6–10] Since the discovery by Fujishima and Honda[11] in 1972 that demonstrated the solar water splitting process, TiO_2 has been extensively investigated for its earth abundance, non-toxicity and good stability in solution.[12–14] However, its theoretical solar energy conversion efficiency is quite low because of the large band gap (*i.e.*, 3.0–3.2 eV) which limits the sunlight absorption to the UV section of the solar spectrum.[15,16] With a direct band gap of 2 eV, and thus with a theoretical 18% solar-to-fuel conversion efficiency, p-type Cu_2O is an attractive photocathode material for photoelectrochemical hydrogen production.[17] Even so, Cu_2O at present cannot in practice be used because of its poor stability when used for water splitting. In fact, this photocorrosion problem is common for the narrow band gap semiconductors (*i.e.*, E_g < 2 eV) in the electrolyte; this is because their self-reduction/oxidation potential level lies more positively/negatively than the water reduction/oxidation potential level. To overcome this corrosion limitation, thin TiO_2 film has recently been deposited onto Cu_2O film, gaining both visible light absorption and improved system stability.[18] On the other hand, while the diffusion length of the minority carriers (electrons) for Cu_2O film (less than 100 nm) is not compatible with the absorption length of light (*i.e.*, 2.2 μm),[19] structures based on Cu_2O nanowire arrays offer the possibility of solving this conflicting demand between light absorption and charge carrier collection.[20] In fact, the array of vertically aligned nanowires provides a high surface area and thus a fast channel for the transfer of photoelectrons to across the nearby surface to the electrolyte before recombination.[21–23]

In this work, we prepared copper oxide nanowire arrays by oxidizing Cu nanowires electrodeposited onto Au substrates. The process was low-cost and scalable. By controlling the oxidation temperature and time, highly aligned Cu_2O nanowires and Cu_2O/CuO core/shell structures were successfully fabricated. Photoelectrochemical measurements were carried out to study their activity and stability, and the CuO shell was found to increase the photoresponse of the photoelectrode and prevent the photocorrosion of the Cu_2O light absorber layer. With a subsequent growing of the TiO_2 coating layer, the photocurrent and stability of the photocathode were further enhanced. The mechanism for the improved performance by the $Cu_2O/CuO/TiO_2$ configuration was investigated through a detailed characterization and analysis on its structure, circuitry and band alignment.

[a]Department of Physics, The Chinese University of Hong Kong, Shatin, New Territory, Hong Kong, China. E-mail: xdxiao@phy.cuhk.edu.hk; Fax: +852 2603-5204; Tel: +852 3943-4388

[b]Shenzhen Institute of Advanced Technology, Chinese Academy of Science, Shenzhen, China

Experimental

Synthesis of photocathodes

The Cu nanowires array was synthesized *via* electrodepostion by using Anodic Aluminum Oxide (AAO) templates (Whatman, 20 nm pore size, 60 μm thick, Anodisc 13), based on the procedure described in ref. 24. In brief, an Au disc (1 cm × 1 cm, 0.5 mm thick, 99.9% Au) which formed ohmic contact with Cu_2O was used as the substrate. The two-electrode electrodeposition cell configuration is shown in Fig. 1. The cell was manufactured by stacking Cu foil (electric conductor for Au cathode), Au substrate (cathode), AAO template, cellulose membrane paper (Whatman) and a Cu anode one-by-one and then sandwiching them between two synthetic glass plates. Before electrodeposition, the Au substrate was mechanically polished with 1 μm alumina slurry and then ultrasonically cleaned in ethanol followed by rinsing with DI water. This process was important to obtain uniform and non-peeling nanowire arrays. The electrodepostion bath was prepared by dissolving 5 g $CuSO_4 \cdot 5H_2O$ (Alfa Aesar), 1 g $(NH_4)_2SO_4$ (Alfa Aesar) and 4 mL diethyl-triamine (DETA, Alfa Aesar) in 50 mL DI water. Alternative cathodic currents (-3 mA cm^{-2} for 0.25 s; -15 mA cm^{-2} for 0.05 s) over 20 minutes were used to electrodeposit Cu nanowires onto the Au substrate after prior soaking in electrolyte for at least 10 minutes. After electrodeposition, the Au cathode was immersed into 2 M NaOH solution for 1 hour to remove the AAO templates and then rinsed with DI water.

The copper oxide nanowires were prepared by thermal oxidation of copper nanowires on a hot plate in air. The Cu nanowires were annealed in air firstly at 150 °C for 30 minutes to form Cu_2O nanowires, followed by further annealing at 180 °C for 1 hour to form Cu_2O/CuO core/shell nanowires. The pure CuO nanowire control sample was prepared by annealing the Cu nanowire at 300 °C for 3 hours and the Cu_2O film control sample was fabricated by annealing an electrodeposited Cu film with the electrodeposition (except without AAO template) and annealing conditions kept the same as for the Cu_2O nanowires.

TiO_2 was deposited on the Cu_2O/CuO nanowires by dip coating. The coating solution was 0.5 mL titanium butoxide (Sigma Aldrich) in 20 mL ethanol. The Cu_2O/CuO nanowires array obtained by oxidation at 180 °C for 30 minutes in air was immersed into the solution for 1 minute and then withdrawn at a speed of 1 mm s^{-1}, followed by air drying for 1 minute at room temperature. The dipping process was carried out 30 times, and then the sample was calcined at 180 °C for 30 minutes. The Cu_2O/TiO_2 core/shell sample was prepared by oxidizing Cu nanowires with the same TiO_2 coating at 150 °C for 30 minutes.

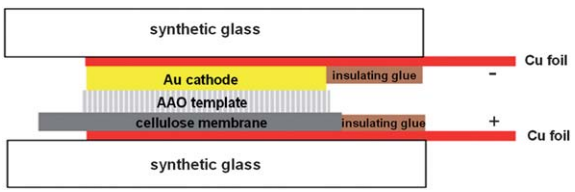

Fig. 1 Electrochemical cell for the synthesis of the Cu nanowire arrays.

Here, the titanium butoxide/ethanol ratio was found to be critical for obtaining TiO_2 uniform coating layers. When the titanium butoxide concentration was too high, TiO_2 would accumulate into islands.

Structural characterization and photoelectrochemical measurements

The morphology of the nanowire arrays was observed by scanning electron microscopy (SEM; Quanta 400; FEI) and their crystal structure was studied by an X-ray diffractometer (Smart Lab; Rigaku). The microstructure and chemical composition of nanowires were investigated by transmission electron microscopy (TEM; Tecnai Model F20; FEI). X-ray photoelectron spectroscopy (XPS) data was collected by PHI Quantum 2000 under ultrahigh vacuum ($<10^{-8}$ torr). The photoelectrochemical performance of the photocathodes was evaluated with a standard electrochemical workstation (CHI660C) in the three-electrode configuration. The counter electrode was a Pt wire and the reference electrode was an Ag/AgCl electrode in saturated KCl. 1.0 M Na_2SO_4 solution buffered at pH 4.9 was used as the electrolyte. In the electrochemical impedance spectroscopy (EIS) measurement, the Nyquist plots were scanned at an AC amplitude of 5 mV with a frequency ranging from 10^5 Hz to 0.08 Hz and the fixed frequency of the M–S plots was 10^3 Hz. The light source was a 300 W Xe lamp equipped with an ultraviolet filter and the light intensity was calibrated with a Si diode to simulate AM 1.5 illumination (1000 W m^{-2}). The linear sweep voltammetry was scanned at a rate of 10 mV s^{-1} and the stability test under chopped light (light on/off cycles: 10 s) was carried out at the fixed potential of 0 V *versus* RHE for 20 minutes.

Results and discussion

Structural characterization of nanowire arrays based photocathodes

With scanning electron microscopic (SEM) images, Fig. 2a shows the morphology of the arrayed Cu nanowires. The average diameter of the Cu nanowires was about 160 nm, which is much larger than the nominal 20 nm AAO pore diameter. In fact, the diameters of the AAO pores near the surface were made wider by the etching process during template manufacture, and only these widened parts were used here to restrict the diameter of the Cu nanowires (this is because the nanowire length was only about 3 μm (Fig. 2d)). The copper oxide nanowires were fabricated by thermal oxidation of the copper nanowires on a hot plate in air. After the first stage of thermal oxidization at 150 °C, the diameters of the nanowires became larger and their surfaces became slightly rougher (Fig. 2b), as compared to the as-grown Cu nanowires. Oxidation at 180 °C for 1 hour further inflated the nanowires and roughened their surfaces (Fig. 2c), while the array structure was largely maintained. As the nanowires' surfaces were more easily oxidized because of the easier access to oxygen, the above procedures were speculated to form Cu_2O/CuO core/shell nanowire microstructures.[25] After the deposition of TiO_2 on Cu_2O/CuO nanowires by dip coating, the surfaces of the nanowires became smoother (Fig. 2f). The

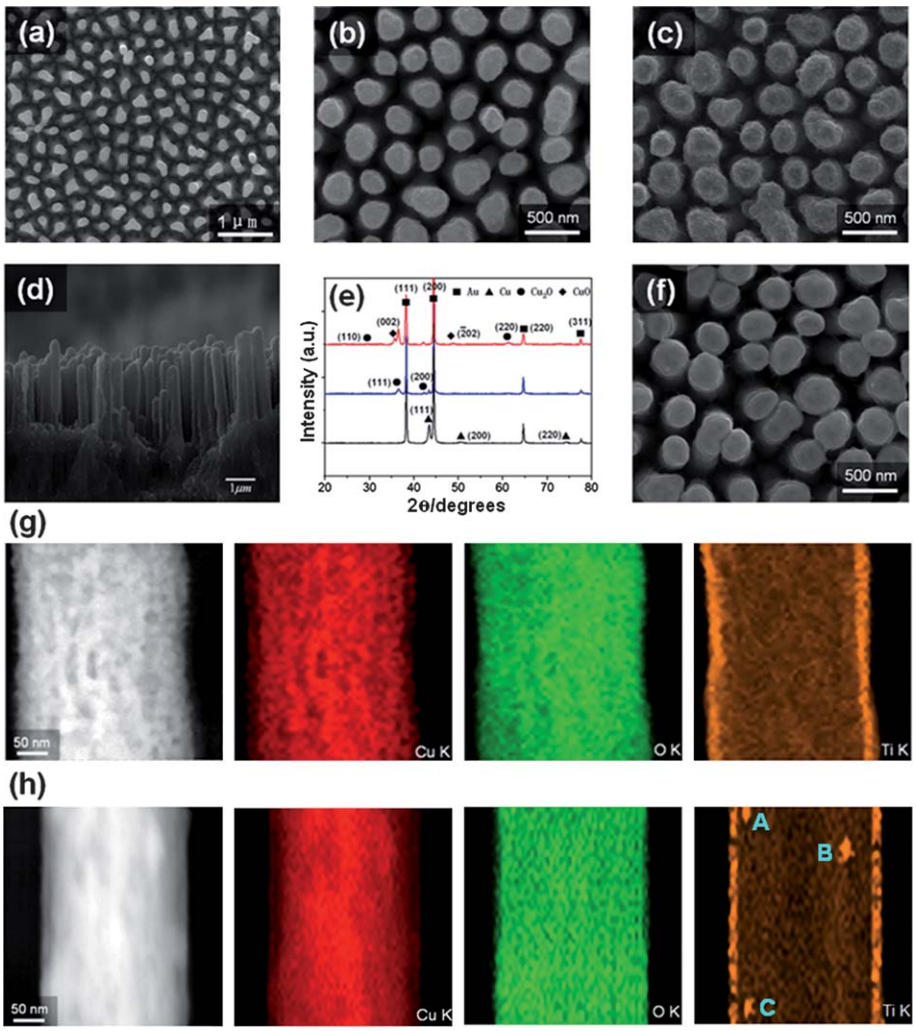

Fig. 2 Characterization of different nanowires. SEM images of (a) Cu, (b) Cu_2O, (c and d) Cu_2O/CuO and (f) Cu_2O/CuO/TiO_2 on Au substrates. (e) X-ray diffraction (XRD) patterns of (a), (b) and (c). STEM image and corresponding EDX elemental mapping of Cu, O and Ti of a single Cu_2O/CuO/TiO_2 nanowire (g) and Cu_2O/TiO_2 nanowire (h).

scanning transmission electron microscope (STEM)-energy dispersive X-ray spectroscopy (EDX) elemental mapping (Fig. 2g) shows a layer of ~10 nm thick TiO_2 on the surface of the Cu_2O/CuO nanowires. In contrast, Fig. 2h shows that the TiO_2 layer in the Cu_2O/TiO_2 configuration was less uniform, with the brighter spots in the Ti elemental mapping (labeled A, B and C) showing the aggregation of TiO_2 and the darker spots along the interface of Cu_2O and TiO_2 showing the uncovered Cu_2O surface. We speculated that the CuO layer provided a better surface for TiO_2 growth.

The formation of the Cu_2O and Cu_2O/CuO nanowires at different annealing stages was suggested by the X-ray diffraction (XRD) patterns shown in Fig. 2e. Fig. 3 further compares the changes of crystallinity of the nanowires before and after annealing at 180 °C by using TEM. Whereas the ring diffraction pattern of the selected area electron diffraction (SAED) contained only those from polycrystalline Cu_2O after the first-stage annealing at 150 °C (Fig. 3b), diffractions from CuO appeared after further annealing at 180 °C (Fig. 3e). In addition, the sharpened ring patterns with obvious diffraction spots revealed the formation of larger Cu_2O grains. Using the EDX line-scanning in STEM to probe the spatial distribution of the Cu and O compositions across a single nanowire, we further confirmed the formation of the Cu_2O/CuO core/shell microstructure. While the Cu : O atomic ratio of the Cu_2O nanowire was nearly 2 : 1 at all positions across the nanowire diameter (Fig. 3c), the Cu : O ratio of Cu_2O/CuO nanowire firstly held steady at about 1 : 1 near the surface, indicating a CuO shell and then gradually increased to around 1.9 : 1 towards the inside (Fig. 3f), consistent with a Cu_2O core and a 15 nm thick CuO shell.

Photoelectrochemical measurements of different photocathodes

Fig. 4a shows the current–potential curves of different photocathodes under chopped AM 1.5 light illumination to study their photoelectrochemical response. The cathodic photocurrent feature of the photoelectrodes confirmed that the Cu_2O was

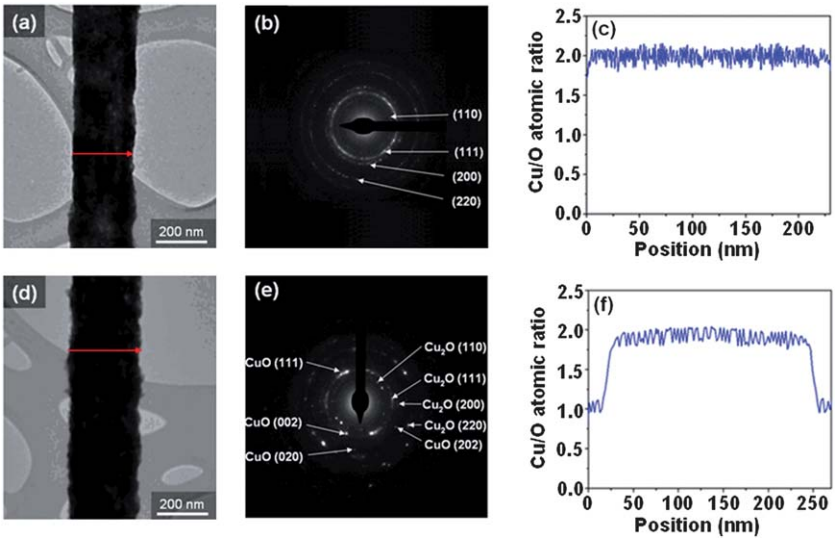

Fig. 3 TEM images and SAED patterns of (a and b) Cu_2O nanowire and (d and e) Cu_2O/CuO nanowire. (c) and (f) show the Cu/O atomic ratio extracted from STEM along the diameter of the nanowires (indicated by the red arrows in the STEM image) of Cu_2O and Cu_2O/CuO nanowires respectively.

p-type. The Cu_2O nanowire arrays generated a photocurrent of 0.50 mA cm^{-2} at 0 V *versus* reversible hydrogen electrode (RHE), which was about twice that of the Cu_2O film control sample. Hwang *et al.* also reported this improvement of nanowire arrays over the film structure by showing that the anodic photocurrent of Si/TiO_2 core/shell nanowire arrays was 2.5 times that of planar Si/TiO_2.[16] The array of nanowires had a higher photocurrent mainly because of the facilitation of the fast transfer of photon-excited electrons to the electrolyte to reduce the recombination inside the semiconductor; this is particularly helpful in a semiconductor with a short minority carrier diffusion length, such as Cu_2O.[19] The cathodic photocurrent density was enhanced to 0.70 mA cm^{-2} after the growth of the CuO layer onto the nanowires, and further improved to 0.87 mA cm^{-2} after additional TiO_2 coating. Moreover, the CuO/TiO_2 layers also positively shifted the onset potential of the cathodic photocurrent by 140 mV. Similar phenomena were found in the $CuGa_3Se_5$ photocathode coated with ZnS by chemical bath deposition (CBD).[26] This photoactivity improvement by the Cu_2O/CuO heterojunction, further completed by the TiO_2 layer, was due to the enhanced separation of electron–hole pairs and the reduced carrier recombination by decreased interface defects.

Fig. 4b shows the results of photocurrent stability of different photocathodes in chopped light. After a 20 minute test at 0 V *versus* RHE, the remnants of photocurrent (the ratio of the photocurrent density at the end of the last light cycle to that at the end of the first light cycle) for Cu_2O, Cu_2O/CuO, Cu_2O/CuO/TiO_2 and Cu_2O/TiO_2 were 8%, 30%, 44% and 31%, respectively. This demonstrated that the growth of the CuO and TiO_2 protecting layers strongly enhanced the stability of the photoelectrodes. Previous work by Grätzel's group, concerning an electrodeposited Cu_2O film protected with ZnO and TiO_2 layers grown by atomic layer deposition also showed an improved photocathode performance.[17] Nonetheless, here we used the much simpler dip coating process to synthesize the TiO_2 protecting layer. After further optimization of this deposition procedure for the ultra-thin layer and improvement of the

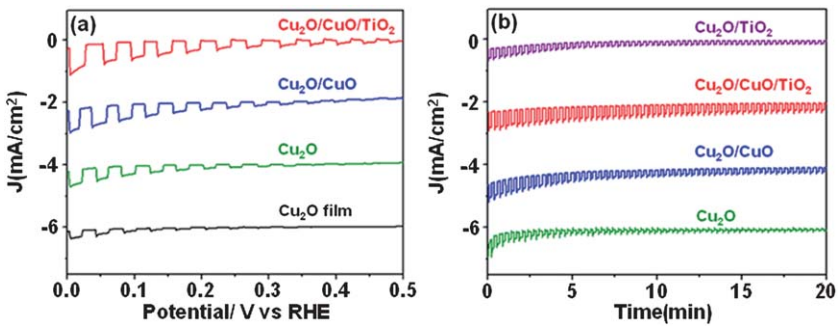

Fig. 4 The photoelectrochemical response of different photocathodes. (a) Current–potential curves of Cu_2O film and different nanowire arrays under chopped AM 1.5 light measured in 1.0 M Na_2SO_4 electrolyte buffered at pH 4.9. The curves of Cu_2O film (black line), bare Cu_2O (green line) and Cu_2O/CuO (blue line) are shifted vertically for clarity. (b) Current–time curves of different nanowire arrays held at 0 V *versus* RHE in chopped light for the stability test. The curves of bare Cu_2O (green line), Cu_2O/CuO (blue line) and Cu_2O/CuO/TiO_2 (red line) are shifted vertically for clarity.

crystalline quality for Cu_2O nanowires in the future, the photocathodes may have the advantages of both high photoresponse and low cost.

The factors affecting the photocathodes' stability

The very unstable photocurrent observed in the case of the bare Cu_2O nanowire arrays was mainly due to its self-reduction by the photon-excited electrons. The red curves in Fig. 5a shows the Auger Cu LMM spectra of Cu_2O nanowires before and after the stability test. A peak of kinetic energy at 918.5 eV, which corresponds to the Cu(0) state, appeared after the test. This confirmed that the surface of the bare Cu_2O was reduced to Cu during the 20 minute photocathodic test. On the other hand, no peak related to Cu(0) emerged in the Cu LMM spectra of Cu_2O/CuO after the stability test (blue curves in Fig. 5a), revealing the protection role of the CuO layer for the Cu_2O core.

The limited stability enhancement of the Cu_2O/CuO photocathode (Fig. 4b, blue curve) stimulates us to examine the reasons behind it. The Cu 2p core level XPS spectra in Fig. 5b and c were used to show the surface change after the stability test. The two binding energy peaks located at 933.5 and 953.2 eV were assigned to Cu $2p_{3/2}$ and Cu $2p_{1/2}$ of CuO, respectively, and the two smaller fitting peaks at 932.4 and 952.2 eV were assigned to Cu_2O. The two extra shake-up satellite peaks further illustrated the existence of CuO. After the stability test, only the binding energy peaks related to Cu $2p_{3/2}$ and Cu $2p_{1/2}$ of Cu_2O remained in the XPS spectra (Fig. 5c), thereby indicating the corrosion of the protecting layer of CuO itself. This result was consistent with the Cu LMM spectra in Fig. 5a (blue line) which showed that the Cu LMM peak shifted from 917.1 eV to 916.6 eV (corresponding to Cu_2O) after the stability test. Thus, the CuO layer of the Cu_2O/CuO photocathode was reduced to Cu_2O during the test. As a comparison, CuO was found to be preserved in the Cu_2O/CuO/TiO_2 photocathode (Fig. 5d) after the stability test, showing that Cu_2O/CuO was protected from photocorrosion by the TiO_2 coating layer. Nevertheless, Fig. 5e showed the Ti $2p_{3/2}$ and Ti $2p_{1/2}$ XPS peaks of TiO_2 located at 458.8 eV and 464.4 eV respectively. After the stability test, a broader shoulder around 456 eV was found in the Ti 2p XPS spectra, revealing the reduction of Ti^{4+} into Ti^{3+}, which explained the photocurrent decrease (although being much smaller than the bare Cu_2O) in this case (Fig. 4b, red curve).

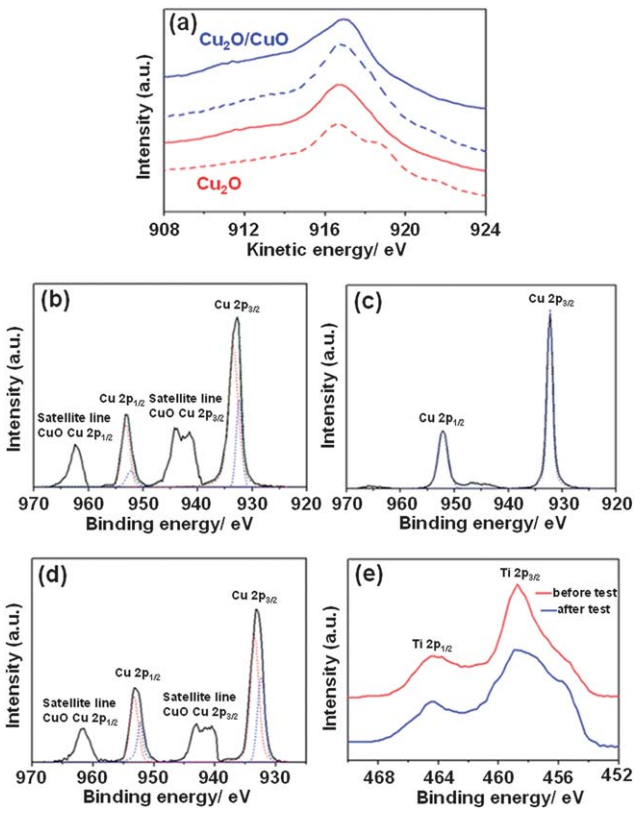

Fig. 5 Results of a 20 minute stability test: (a) Auger Cu LMM spectra of Cu_2O/CuO before (blue line) and after (blue dashed line), bare Cu_2O before (red line) and after (red dashed line) the stability test. (b) and (c) XPS Cu 2p spectra of Cu_2O/CuO before and after the stability test. (d) Cu 2p spectra of Cu_2O/CuO/TiO_2 after the stability test. (e) Ti 2p spectra of Cu_2O/CuO/TiO_2 before and after the stability test.

The advantages of Cu_2O/CuO/TiO_2 configuration

To reveal the reasons of the advantageous Cu_2O/CuO/TiO_2 configuration over others, electrochemical impedance spectroscopy (EIS) was used to study the electrochemical properties of the photoelectrodes. The semicircular features of the Nyquist plots (Fig. 6) indicated that the photoelectrode/electrolyte interface could be regarded as a circuit of a resistor and a capacitor in parallel. The diameter of the semicircle was equal to the resistance R of the charge transfer. For all the photocathodes the resistance under light was much lower than that in the dark because of the higher charge carrier densities induced by photo-excitation. The Cu_2O/CuO/TiO_2 configuration had the lowest resistance both in dark and under illumination, which illuminated that this structure could better facilitate the electron transfer from the photoelectrode to the electrolyte and thus

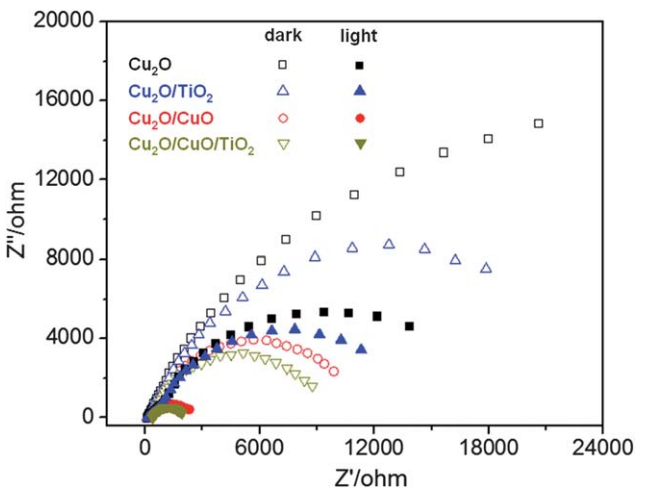

Fig. 6 Nyquist plots of Cu_2O, Cu_2O/CuO and Cu_2O/CuO/TiO_2 nanowire arrays based photocathodes both in dark and under AM 1.5 illumination in 1.0 M Na_2SO_4 electrolyte buffered at pH 4.9.

explained that it had the best photoresponse and best stability as described above.

To investigate the band alignment and thus the charge transfer between Cu_2O and CuO prepared by thermal oxidation of copper nanowires, the Mott–Schottky (M–S) plots of pure Cu_2O and pure CuO nanowire arrays (Fig. 7) based on equation:

$$\frac{1}{C^2} = \frac{2}{\varepsilon_0 \varepsilon_r e N_A}\left(V - V_{fb} - \frac{k_B T}{e}\right) \quad (1)$$

were used to determine their flat band potential V_{fb} and charge carrier density N_A. Here, C is the space-charge capacitance of the semiconductor; ε_0 is the permittivity in vacuum; ε_r is the dielectric constant; V is the applied potential and T is the temperature. From the linear fit of $1/C^2$ *versus* V, V_{fb} for Cu_2O and CuO was obtained to be 0.82 eV and 0.74 eV *vs.* RHE respectively, while the hole concentration N_A for Cu_2O and CuO was 3.8×10^{17} cm^{-3} and 3.9×10^{18} cm^{-3} respectively (ε_r of Cu_2O and CuO were taken as 7.6 and 18.1 respectively[27,28]). The valence band edge E_V could be obtained according to:

$$E_V = E_F - k_B T \ln \frac{N_V}{N_A} \quad (2)$$

where $N_V = 2\frac{(2\pi m_p^* k_B T)^{3/2}}{h^3}$. As the effective mass m_p^* of the holes was $0.58m_0$ for Cu_2O and $7.9m_0$ for CuO,[29,30] the effective density of states N_V of the valence band for Cu_2O and CuO were 1.11×10^{19} cm^{-3} and 5.57×10^{20} cm^{-3} respectively. The valence band edge E_V for Cu_2O and CuO was then calculated to be 0.91 eV and 0.87 eV *vs.* RHE, both of them were in agreement with previous results.[19,31]

Considering the respective band gaps of 2.0 eV and 1.56 eV for Cu_2O and CuO,[17,31,32] the band alignment diagram of Cu_2O/CuO/TiO_2 in contact with the electrolyte was shown in Fig. 8. The nanowire arrays reached equilibrium with the electrolyte in the dark which resulted in an upward shift of the band level of the Cu_2O core due to the built-in electric field caused by the space charge layer at the Cu_2O/CuO/TiO_2 nanowire electrolyte interface. In the photoelectrochemical process, the photon-excited electrons in Cu_2O under illumination were channelled to the TiO_2/electrolyte interface through the conduction band of CuO and TiO_2 successively, while the holes were transferred to the Pt counter electrode through the Au substrate and the external circuit (some hole trapping may also occur at the CuO shell, unfortunately). The TiO_2 layer formed a p–n junction with the inner Cu_2O/CuO. As the lattice constant for TiO_2 ($a = 0.458$ nm) and Cu_2O ($a = 0.427$ nm) was highly mismatched, which effectively prevented the direct conformal growth of TiO_2 on Cu_2O, as demonstrated by the Ti elemental mapping in Fig. 2h, and the poor performance of the Cu_2O/TiO_2 photocathode, the CuO ($a = 0.468$ nm) had a much reduced lattice mismatch with TiO_2 and had provided a better interface for TiO_2 growth. It was surprising that the interface between CuO and Cu_2O with a large lattice mismatch had not resulted in a strong negative effect, most likely because of the peculiar growth mode that might provide a gradual composition change along the radial direction of the nanowires as shown in Fig. 3f. This gradual composition change of the Cu_2O surface into CuO resulted in a graded band gap at the interface between Cu_2O and CuO. The band bending resulted from the p–n junction together with the large drift field ($\sim 5 \times 10^5$ V cm^{-1}; 0.5 eV change of the conduction band in the 10 nm thick graded composition layer) resulting from the graded conduction band[33] could have assisted the electron–hole pair separation and the transfer of electrons to the interface of the photocathode and electrolyte. With a plausible better interface as described above, a reduced charge depletion region due to a high doping concentration N_A in CuO (one order of magnitude larger than that in Cu_2O), and an

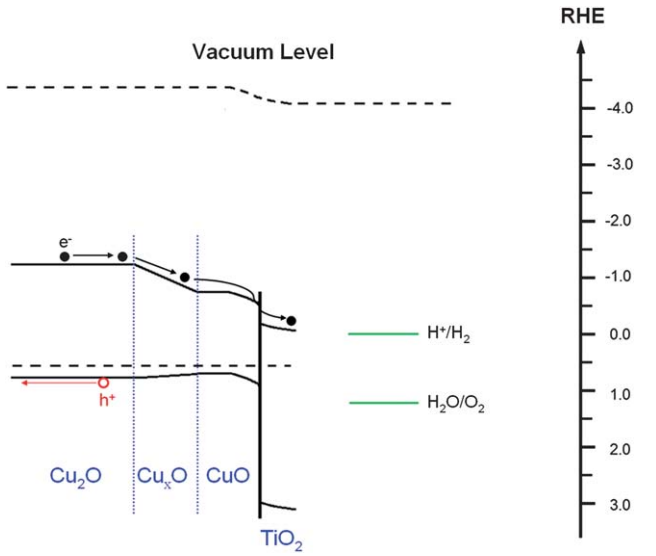

Fig. 8 Energy band diagram and charge transfer for Cu_2O/CuO/TiO_2 in 1.0 M Na_2SO_4 electrolyte in the dark (buffered at pH 4.9).

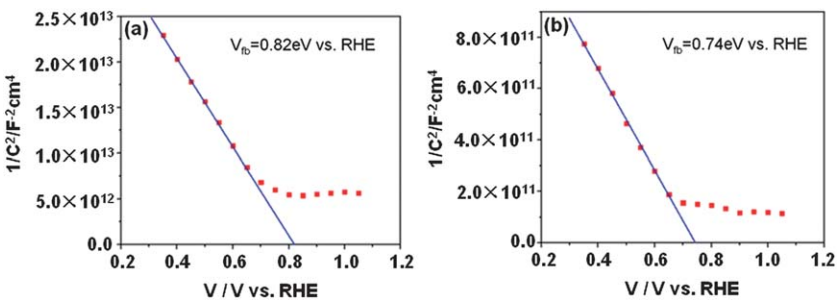

Fig. 7 Mott–Schottky plots of Cu_2O (a) and CuO (b) photocathodes.

indirect band gap in nature,[34] the introduction of a CuO layer into the $Cu_2O/CuO/TiO_2$ structure could immensely reduce the recombination of the electrons and holes within the charge depletion region. For a radial p–n junction nanowires based device, the recombination in the depletion region was identified to affect the photoresponse more than that in the quasi-neutral region.[35] Thus, the CuO layer, in addition to the TiO_2 layer in the $Cu_2O/CuO/TiO_2$ configuration, played important roles to obtain the best performance compared with other photocathodes as shown in Fig. 4. The band diagram in Fig. 8 also pointed out that the function of the protection layers was limited because that the TiO_2 Fermi level was still not energetic enough for electrons to rapidly transfer to the electrolyte, resulting in the self-reduction of Ti^{4+} to Ti^{3+}, as suggested by the Ti 2p XPS spectra (Fig. 5e).[17] In future work, we plan to deposit co-catalysts (such as Pt nanoparticles with diameters of several nanometers),[5] which are efficacious in reducing the water reduction barrier and avoiding the reduction of any layer in the photocathodes.

Conclusions

We have successfully fabricated Cu_2O, Cu_2O/CuO, $Cu_2O/CuO/TiO_2$, and Cu_2O/TiO_2 nanowire arrays on Au substrates. The photocurrent of the Cu_2O nanowire arrays was twice that of the Cu_2O film as a result of the nanowires configuration which decoupled the conflicting demand between the light absorption and the charge carrier collection. Among the different nanowire array photocathodes, the $Cu_2O/CuO/TiO_2$ configuration showed the best photoresponse and stability. This core/shell nanowires array not only provided the outer protecting layers to shield Cu_2O core from direct contact with the electrolyte and inhibit its photocorrosion, but also facilitated the effective separation of electrons and holes and the effective reduction of minority carrier recombination, as analyzed by its structure, circuitry and band alignment. It is expected that this material-abundant and easy-manufactured $Cu_2O/CuO/TiO_2$ photocathode has a great potential in practical application. Moreover, this approach with protecting outer layers can also be applied to other narrow band gap semiconductors suffering from photocorrosion to enable more suitable candidates for water photoelectrolysis.

Acknowledgements

This work was supported by the CUHK Group Research Scheme Grant, the CUHK Focused Scheme B Grant "Center for Solar Energy Research", GRF of HKSAR (Project no. 414710) and the National Major Science Research Program of China (Project no. 2012CB933700).

Notes and references

1 M. Halmann, *Nature*, 1978, **275**, 115–116.
2 A. J. Bard, *J. Photochem.*, 1979, **10**, 59–75.
3 D. Gust, T. A. Moore and A. L. Moore, *Acc. Chem. Res.*, 2001, **34**, 40–48.
4 A. Magnuson, M. Anderlund, O. Johansson, P. Lindblad, R. Lomoth, T. Polivka, S. Ott, K. Stensjo, S. Styring, V. Sundstrom and L. Hammarstrom, *Acc. Chem. Res.*, 2009, **42**, 1899–1909.
5 H. Yan, J. Yang, G. Ma, G. Wu, X. Zong, Z. Lei, J. Shi and C. Li, *J. Catal.*, 2009, **266**, 165–168.
6 A. J. Nozik, *Annu. Rev. Phys. Chem.*, 1978, **29**, 189–222.
7 O. Khaselev and J. A. Turner, *Science*, 1998, **280**, 425–427.
8 Y. Q. Wang, Z. J. Zhang, Y. Zhu, Z. C. Li, R. Vajtai, L. J. Ci and P. M. Ajayan, *ACS Nano*, 2008, **2**, 1492–1496.
9 M. G. Walter, E. L. Warren, J. R. Mckone, S. W. Boettcher, Q. Mi, E. A. Santori and N. S. Lewis, *Chem. Rev.*, 2010, **110**, 6446–6473.
10 S. Y. Reece, J. A. Hamel, K. Sung, T. D. Jarvi, A. J. Esswein, J. H. Pijpers and D. G. Nocera, *Science*, 2011, **334**, 645–648.
11 A. Fujishima and K. Honda, *Nature*, 1972, **238**, 37–38.
12 J. Nowotny, T. Bak, M. K. Nowotny and L. R. Sheppard, *Int. J. Hydrogen Energy*, 2007, **32**, 2609–2629.
13 I. S. Cho, Z. B. Chen, A. J. Forman, D. R. Kim, P. M. Rao, T. F. Jaramillo and X. L. Zheng, *Nano Lett.*, 2011, **11**, 4978–4984.
14 J. C. Yu, L. Wu, J. Lin, P. S. Li and Q. Li, *Chem. Commun.*, 2003, 1552–1553.
15 A. L. Linsebigler, G. Q. Lu and J. T. Yates, *Chem. Rev.*, 1995, **95**, 735–758.
16 Y. J. Hwang, A. Boukai and P. D. Yang, *Nano Lett.*, 2009, **9**, 410–415.
17 A. Paracchino, V. Laporte, K. Sivula, M. Grätzel and E. Thimsen, *Nat. Mater.*, 2011, **10**, 456–461.
18 W. Siripala, A. Ivanovskaya, T. F. Jaramillo, S. H. Baeck and E. W. McFarland, *Sol. Energy Mater. Sol. Cells*, 2003, **77**, 229–237.
19 A. Paracchino, J. C. Brauer, J. E. Moser, E. Thimsen and M. Grätzel, *J. Phys. Chem. C*, 2012, **116**, 7341–7350.
20 A. I. Hochbaum and P. D. Yang, *Chem. Rev.*, 2010, **110**, 527–546.
21 X. N. Wang, J. Wang, M. J. Zhou, H. J. Zhu, H. Wang, X. D. Cui, X. D. Xiao and Q. Li, *J. Phys. Chem. C*, 2009, **113**, 16951–16953.
22 M. J. Zhou, H. J. Zhu, X. N. Wang, Y. M. Xu, Y. Tao, S. K. Hark, X. D. Xiao and Q. Li, *Chem. Mater.*, 2010, **22**, 64–69.
23 X. N. Wang, H. J. Zhu, Y. M. Xu, H. Wang, Y. Tao, S. K. Hark, X. D. Xiao and Q. Li, *ACS Nano*, 2010, **4**, 3302–3308.
24 P. L. Taberna, S. Mitra, P. Poizot, P. Simon and J. M. Tarascon, *Nat. Mater.*, 2006, **5**, 567–573.
25 S. Han, H. Y. Chen, Y. B. Chu and H. C. Shih, *J. Vac. Sci. Technol., B*, 2005, **23**, 2557–2560.
26 J. Kim, T. Minegishi, J. Kobota and K. Domen, *Energy Environ. Sci.*, 2012, **5**, 6368–6374.
27 Z. H. Zhang and P. Wang, *J. Mater. Chem.*, 2012, **22**, 2456–2464.
28 R. L. David, *CRC Handbook Chemistry and Physics, 85th*, 2004, pp. 12–54.
29 J. W. Hodby, T. E. Jenkins, C. Schwab, H. Tamura and D. Trivich, *J. Phys. C: Solid State Phys.*, 1976, **9**, 1429–1440.

30 F. P. Koffyberg and F. A. Benko, *J. Appl. Phys.*, 1982, **53**, 1173–1177.
31 K. Nakaoka, J. Ueyama and K. Ogura, *J. Electrochem. Soc.*, 2004, **151**, C661–C665.
32 C. Y. Chiang, K. Aroh, N. Franson, V. R. Satsangi, S. Dass and S. Ehrman, *Int. J. Hydrogen Energy*, 2011, **36**, 15519–15526.
33 K. Makoto and T. Kiyoshi, *J. Appl. Phys.*, 1975, **46**, 3542–3546.
34 D. X. Wu, Q. M. Zhang and M. Tao, *Phys. Rev. B: Condens. Matter Mater. Phys.*, 2006, **73**, 235206.
35 B. M. Kayes, H. A. Atwater and N. S. Lewis, *J. Appl. Phys.*, 2005, **97**, 114302.